

Supplementary Information for Ubiquitous Spin-Orbit Coupling in Iron-Based Superconductors

R.P. Day^{1,2}, G. Levy^{1,2}, M. Michiardi^{1,2}, M. Zonno^{1,2}, F. Ji^{1,2}, E. Razzoli^{1,2}, F. Boschini^{1,2}, S. Chi^{1,2}, R. Liang^{1,2}, P.K. Das^{3,4}, I. Vobornik³, J. Fujii³, D.A. Bonn^{1,2},
W.N. Hardy^{1,2}, I.S. Elfimov^{1,2}, A. Damascelli^{1,2}

¹*Department of Physics and Astronomy, University of British Columbia, Vancouver, BC V6T 1Z1, Canada*

²*Quantum Matter Institute, University of British Columbia, Vancouver, BC V6T 1Z4, Canada*

³*Istituto Officina dei Materiali (IOM)-CNR, Laboratorio TASC, Area Science Park, S.S.14, Km 163.5, I-34149 Trieste, Italy*

⁴*International Centre for Theoretical Physics (ICTP), Strada Costiera 11, I-34100 Trieste, Italy*

1 Calculating Circularly Polarized Spin and Angle Resolved Photoemission Spectroscopy

In conventional ARPES measurements, experimentalists are conscious of the so-called 'matrix element effects' which modulate the spectral intensity, resulting in deviation from the pure one-electron removal spectral function understood to be the underlying object of measurement in photoemission spectroscopy¹. More explicitly stated, this modulation can be understood easily as originating from the dipole matrix element (valid for spatially homogeneous electromagnetic fields) which is central to the intensity as described by Fermi's golden rule:

$$I(\vec{k}, \omega) \propto \sum_i |\langle \psi_f | \Delta | \psi_i \rangle|^2 |A_i(\vec{k}, \omega)|^2 \quad (1)$$

where $|\psi_i\rangle$ and $|\psi_f\rangle$ represent the initial and final state wavefunctions of the photoemitted electron. The sum goes over all initial states, Δ is the dipole operator and $A_i(\vec{k}, \omega)$ is the one-electron removal spectral

function. While convoluted with the details of the experimental configuration, the matrix element factor is a rich source of information, dependent on not only the parity of the states being probed, but also the relative phase within the Bloch wavefunction, itself taken to be a linear combination of orthonormal atomic orbitals. It is this factor which makes it possible to probe spin-orbital coupling via CPS-ARPES. By working in the Coulomb gauge and neglecting higher-order terms, we can approximate $\Delta = \vec{A} \cdot \vec{p}$, and on the basis that the initial and final states are eigenstates, we can employ the commutation relation $[H, \vec{r}] = \frac{\omega \vec{p}}{c}$ to recast equation (1) in terms of the position operator, such that $\Delta \propto \hat{\epsilon} \cdot \vec{r}$, with $\hat{\epsilon}$ here the polarization unit vector of the incoming light. Following the well-known dipole selection rules, under the dipole operator $\Delta l = \pm 1$ and $m'_l = m_l + \mu$ with $\mu \in [-1, 1]$. These rules are made more explicit by expanding the dipole operator as written in terms of spherical harmonics:

$$\sum_{\mu} \left(\frac{\epsilon_x + i\epsilon_y}{\sqrt{2}} \delta_{\mu,-1} + \epsilon_z \delta_{\mu,0} + \frac{-\epsilon_x + i\epsilon_y}{\sqrt{2}} \delta_{\mu,1} \right) |\vec{r}| Y_{1,\mu}(\theta, \phi) \quad (2)$$

where $Y_{l,m}(\theta, \phi)$ are the usual spherical harmonics. For circularly polarized light however, these rules are further constrained, and this will form the basis of this experimental technique. In the simplest case, light is considered incident normal to the sample surface, such that the polarization plane is spanned by the vectors $\sigma = [1, 0, 0]$ and $\pi = [0, 1, 0]$. Then for circularly polarized light, the polarization vectors are $C_{\pm} = \pi \pm i\sigma$. Substituting this vector into equation 2 we find that under C_+ , $\Delta m_l = 1$ and C_- , $\Delta m_l = -1$. As noted in the text, these strict rules are relaxed off normal incidence, and for the case here, where the polarization vector basis is defined by $\sigma = [1, 0, 0]$ and $\pi = [0, \frac{1}{\sqrt{2}}, -\frac{1}{\sqrt{2}}]$, then the expansion in Equation 1 reduces instead to

$$\sum_{\mu} (0.15 \delta_{\mu,-1} - 0.5 \delta_{\mu,0} + 0.85 \delta_{\mu,1}) |\vec{r}| Y_{1,\mu}(\theta, \phi) \quad (3)$$

for C_+ and

$$\sum_{\mu} (0.85 \delta_{\mu,-1} + 0.5 \delta_{\mu,0} + 0.15 \delta_{\mu,1}) |\vec{r}| Y_{1,\mu}(\theta, \phi) \quad (4)$$

for C_- . While the effect is diminished, the raising nature of C_+ and lowering of C_- is largely intact, even for such large angles of incidence.

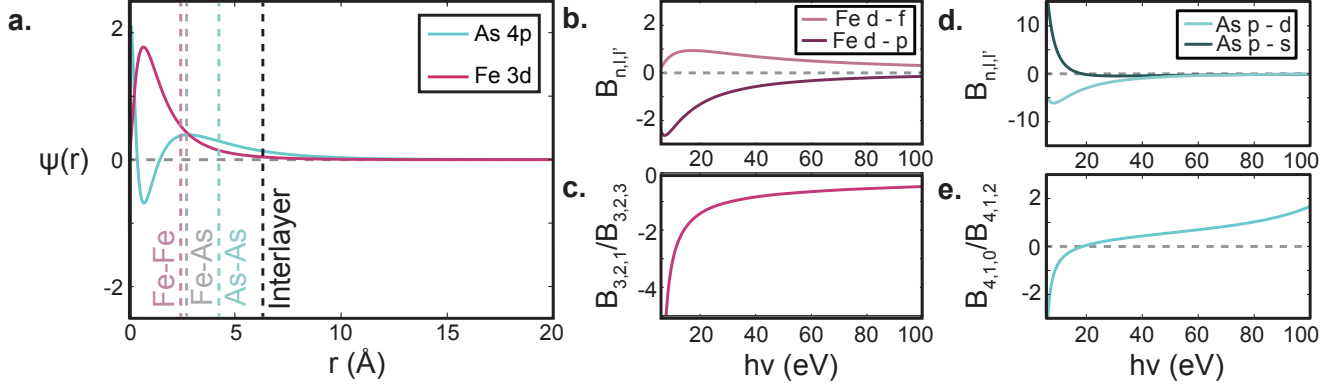


Figure 1 (a) Radial part of the initial state wave functions, taken as the pseudowavefunctions from the Quantum ESPRESSO pseudopotentials for Fe and As. Representative lengthscales for LiFeAs are illustrated with vertical lines showing the distance between nearest Fe-Fe, Fe-As, As-As ions, and the interlayer separation. (b) Radial integrals as in Equation (6) for Fe 3d for dipole transitions into the p and f channels. l and l' reference the orbital angular momentum number for initial and final states respectively. (c) Ratio of the radial integrals into p:f for Fe 3d states. (d-e) same as (b-c) but for the As 4p state going into s and d channels.

This is verified by the simulated plots of P_i (Equation 1 of the main text) in Figure (3b) and (3c) of the main text which show a clear change in sign between states of different spin-orbit coupling polarization, albeit reduced in amplitude from what would be expected for normal incidence light.

In order to simulate ARPES intensity², we begin by making the assumption of a free-electron plane wave final state. We can rewrite the matrix element $M_k = \langle e^{i\vec{k}\cdot\vec{r}} | \hat{\epsilon} \cdot \vec{r} | \psi_i \rangle$ as

$$M_k = 4\pi \sum_{l',m'} B_{n,l,l'}(k) G_{l,m}^{l',m'} Y_{l',m'}(\theta_k, \phi_k) \quad (5)$$

where the radial integral is

$$B_{n,l,l'}(k) = (-i)^{l'} \int dr r^3 j_{l'}(kr) R_{n,l}(r) \quad (6)$$

and the angular integral

$$G_{l,m}^{l',m'} = \sum_{\mu} \left(\frac{\epsilon_x + i\epsilon_y}{\sqrt{2}} \delta_{\mu,-1} + \epsilon_z \delta_{\mu,0} + \frac{-\epsilon_x + i\epsilon_y}{\sqrt{2}} \delta_{\mu,1} \right) \int d\Omega Y_{l,m}(\theta, \phi) Y_{1,\mu}(\theta, \phi) Y_{l',m'}^*(\theta, \phi) \quad (7)$$

Here, primed and unprimed values are used to reference final and initial states, respectively. In constructing the radial integrals, an important question which arises is what should be taken as the radial part of the initial state? While hydrogenic orbitals are excessively localized, Slater-type orbitals lack the radial nodes of real orbitals, and are therefore not necessarily well-founded. Given that Quantum ESPRESSO has been used to generate the Hamiltonian, the electronic pseudowavefunctions from the pseudopotential files has been chosen for the initial states. For the Fe and As atoms used in this paper, the results are plotted in Figure (S1 a). It is instructive to note however that Slater-type orbitals are a good alternative and can be used to similar results. The radial integrals may be calculated over a wide range of photon energies, and the result is plotted in Figure (S1 b-e). This allows for calculation of the ratio with which the electrons undergo transitions from the Fe 3d states to those of 3p and 3f character (Figure S1 c). From this we see that in the range of photon energies used here (25 - 50 eV), transitions into f-channel and p-channel are of similar strength. Similar calculations can be done for the As states, which are not so relevant to the calculations in the main text, however we may confirm that the range of photon energies used are not associated with any dramatic changes in photoemission channels available to the As 4p states (Figure S1 d-e).

We demonstrate here now that the central result of the main text is not qualitatively impacted by the relative strength between transitions into f or p channels. At normal emission and incidence, $Y_{2,1}(\theta, \phi)$ can only photoemit under C_+ into the $Y_{3,2}(\theta, \phi)$ state. However, a node along the normal direction for this harmonic suppresses photoemission via C_+ .

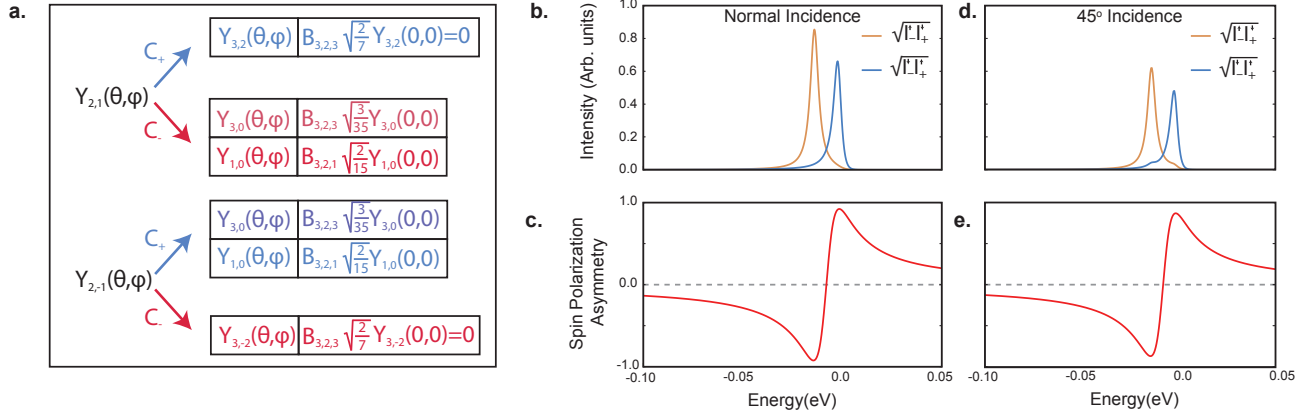


Figure 2 (a) Schematic photoemission amplitude for different initial states and their possible final states under circularly polarized light excitation at normal incidence. The tables indicate the final state spherical harmonics, and their contribution to M_k in the sum of Equation (5). A node in the spherical harmonics $Y_{3,2}(\theta, \phi)$ and $Y_{3,-2}(\theta, \phi)$ precludes photoemission along the normal direction into these states. (b) Simulated EDCs for the two spin-orbit split states at $k_{\parallel} = 0 \text{ \AA}^{-1}$ under normal incident light. The spectral peak is simulated by a Lorentzian of width 5 meV. The electronic temperature is taken as 20 K, as in the experiment. Resolution effects are neglected for sake of clarity. (c) The resulting polarization asymmetry. (d-e) Same as (b-c) but for 45° incident light. Tails in the Lorentzians illustrate the small photoemission intensity from the other state, even for a large angle of incidence.

Consequently, this state can only photoemit via C_- excitation, regardless of relative cross sections for photoemission into p or f final states. Similar arguments can be made for $Y_{2,-1}(\theta, \phi)$ and C_- . As a result, the photoemission at normal emission for these states will constitute a combination of intensity in both the f and p channels. While the quantitative details of the spectra will be dependent on the ratio between these two channels, there is no substantive qualitative impact on the mechanism described within the region of interest, as shown by the smooth variation of $B_{3,2,3} : B_{3,2,1}$ in Figure (S1 b).

In Figure (S2 b) this argument is made more explicit using simulated EDCs, where Lorentzians with

a linewidth of 5 meV and peaks proportional to the matrix elements as summarized by the rules in Figure (S2 a). The relevant spin-polarization asymmetry P is then shown below. In Figure (S2 d-e), the same is done but with the normal incidence condition relaxed, accounting for the true 45° angle of incidence in the experiment. Evidently, the polarization asymmetry is still pronounced, and the concept is not only valid for normal incidence. Only a small additional intensity from the peak we do not intend to address with a given light polarization is observed, manifest by the small tail in the EDCs of Figure (S2d).

Regarding the form of P_i defined in the main text³, Equation (1) is a particularly robust measure of spin-orbit coupling polarization asymmetry as the effects of both circular dichroism and detector efficiency imbalance are eliminated from consideration. If we take the measured intensity $I_{+(-),meas}^{\uparrow(\downarrow)} = D_{\pm} E_{\uparrow(\downarrow)} I_{+(-),true}^{\uparrow(\downarrow)}$, we note then that each term in the numerator and denominator will have $D_+ D_- E_{\uparrow} E_{\downarrow}$ where D_{\pm} and $E_{\uparrow(\downarrow)}$ refer to circular dichroism and detector efficiency respectively. In evaluation of P_i then by Equation (1) of the main text, these factors cancel from the overall expression.

It is instructive to note that the amplitude of the P signal (calculated using Equation (1) of the main text) is much higher than the simulations or measurements in the main text. This is due to both the absence of an incoherent background with no well-defined spin direction, and more importantly resolution effects which leads to much greater overlap of the spectral features than in this schematic model. Furthermore, due to the Sherman function associated with the VLEED detector, the absolute maximum amplitude of the P signal is ± 0.3 . This is an empirical estimate of the fidelity of the spin-target, i.e. the degree to which the target effectively extinguishes the spin-minority photoelectrons diffraction.

2 In-Plane Spin-Polarization Asymmetry

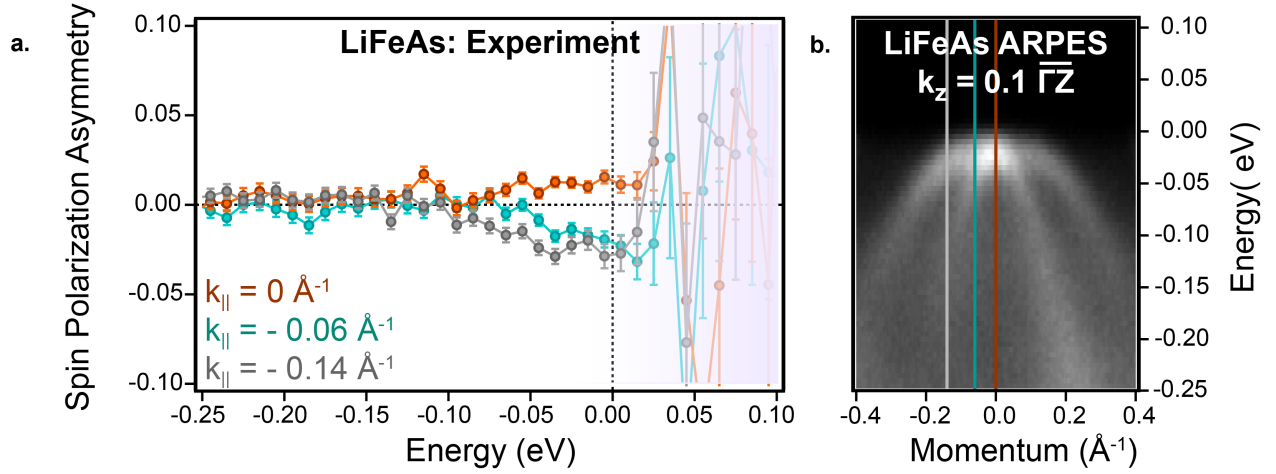


Figure 3 (a) In plane measurements of P_z for LiFeAs (b) ARPES of corresponding region of Brillouin zone studied. A small negative value is observed away from $k_{\parallel} = 0$.

As described in the main text, we measured the in-plane spin projection which is oriented along the axis of the analyzer entrance slit in the experimental configuration. For a crystal oriented with the $\overline{\Gamma M}$ direction parallel to the slit, we acquired spin-EDCs which were used to then generate the spin-polarization asymmetry curves illustrated in Figure (S4). The emission angles for the relevant curves are the same as those for the out of plane measurements in the main text. While the signal is smaller than for the out of plane projection, it would seem that away from normal emission, the spin vectors tilt away from the \hat{z} direction for states near E_F , and no sign of a switch in the sign of P is observed, suggesting P of the same sign on both states for in-plane projection.

3 LiFeAs: Electron Pockets at the Zone Corner

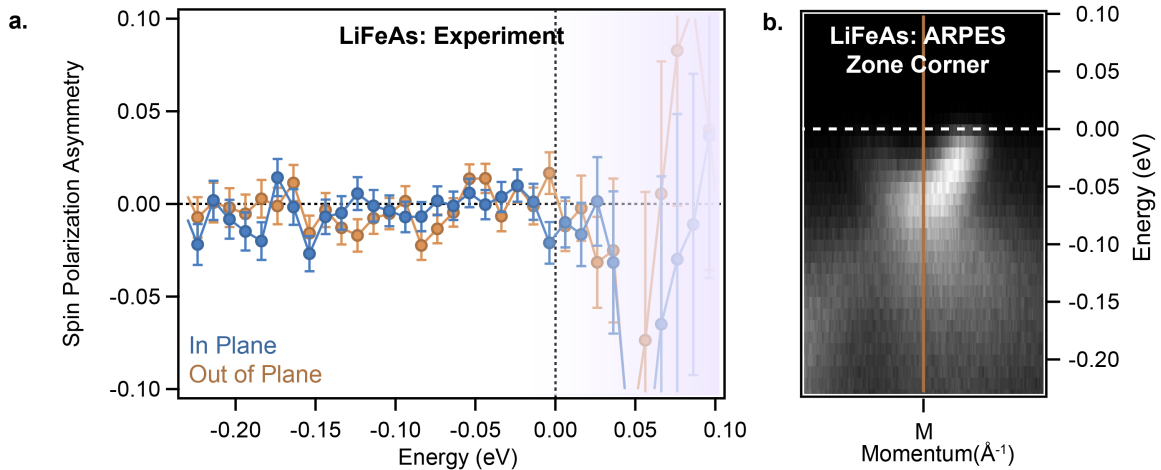


Figure 4 (a) Spin-polarization asymmetry at the zone corner for LiFeAs, as calculated from measured spin-resolved EDCs. (b) Corresponding ARPES spectra at 26 eV for the relevant region of the Brillouin zone. Vertical line indicates the emission angle for the measurements of P_i .

In addition to measurements on the hole pockets at the zone centre, we measured the P_i on the electron pockets at the zone corner for LiFeAs. Both in and out of plane components of spin were measured and P_i calculated, giving the result in Figure (S5 a). The ARPES spectra in Figure (S5 b) indicates the emission angle, which corresponds to the M point of the Brillouin zone. The plot of P_i indicates that as in the case of FeSe, the states at the zone corner do not reflect any substantial coupling of the spin and orbital angular momentum vectors.

1. Damascelli, A. Probing the Electronic Structure of Complex Systems by ARPES. *Physica Scripta* **2004**, 61 (2004). URL <http://stacks.iop.org/1402-4896/2004/i=T109/a=005>.
2. Zhu, Z.-H. *et al.* Layer-By-Layer Entangled Spin-Orbital Texture of the Topological Surface State in Bi_2Se_3 . *Phys. Rev. Lett.* **110**, 216401 (2013). URL <https://link.aps.org/doi/10.1103/PhysRevLett.110.216401>.

3. Veenstra, C. N. *et al.* Spin-Orbital Entanglement and the Breakdown of Singlets and Triplets in Sr_2RuO_4 Revealed by Spin- and Angle-Resolved Photoemission Spectroscopy. *Phys. Rev. Lett.* **112**, 127002 (2014). URL <https://link.aps.org/doi/10.1103/PhysRevLett.112.127002>.